PROCEEDINGS OF SPIE

SPIEDigitalLibrary.org/conference-proceedings-of-spie

# Data reduction for the MIPS far-infrared arrays

Ted Hesselroth, Eng Chong Ha, Misha Pesenson, Doug M. Kelly, G. Rivlis, et al.

Ted Hesselroth, Eng Chong Ha, Misha Pesenson, Doug M. Kelly, G. Rivlis, C. W. Engelbracht, "Data reduction for the MIPS far-infrared arrays," Proc. SPIE 4131, Infrared Spaceborne Remote Sensing VIII, (16 November 2000); doi: 10.1117/12.406570

SPIE.

Event: International Symposium on Optical Science and Technology, 2000, San Diego, CA, United States

# Data reduction for the MIPS far infrared arrays

Ted Hesselroth[a], Eng Ha[a], Misha Pesenson[a], D. Kelly[b], G. Rivlis[b], and C.W. Engelbracht[b]

[a]SIRTF Science Center, Infrared Processing and Analysis Center
California Institute of Technology, MS 100-22, Pasadena, CA 91125
[b]MIPS Project Office, Steward Observatory, University of Arizona, Tucson, Arizona 85721

## ABSTRACT

Traditional photoconductive detectors are used at 70 and 160 microns in the Multiband Imaging Photometer for SIRTF (MIPS).[1] These devices are highly sensitive to cosmic rays and have complex response characteristics, all of which must be anticipated in the data reduction pipeline. The pipeline is being developed by a team at the SIRTF Science Center, where the detailed design and coding are carried out, and at Steward Observatory, where the high level algorithms are developed and detector tests are conducted to provide data for pipeline experiments. A number of innovations have been introduced. Burger's model is used to extrapolate to asymptotic values for the response of the detectors. This approach permits rapid fitting of the complexities in the detector response. Examples of successful and unsuccessful fits to the laboratory test data are shown. A changepoint detector algorithm based on bayesian statistics is implemented for the detection of charge-producing cosmic ray hits in sample-up-the-ramp infrared detector data. The algorithm finds the sample having the maximum likelihood of being a changepoint, and then computes the probability that a changepoint actually occurred at that sample. Tracking the detector calibration with frequent flashes of stimulators in the instrument has been validated for test data. Variations in response to the stimulator have been normalized to a uniform value and applied to all other data. The resulting corrected response was shown to be uniform over a three-hour period of data collection.

**Keywords:** infrared detector, sirtf, space telescope, ipac, nasa, ge:ga, cosmic ray, burger's equation, mips, multiband imaging photometer

## 1. BURGERS EQUATION AND TRANSIENTS IN GALLIUM DOPED GERMANIUM DETECTORS

### 1.1. Derivation of the Burgers equation

Gallium doped germanium detectors have been known to exhibit a number of transient effects under low background conditions. Such behavior creates calibration uncertainties. In this section we will analyze monotonic and nonmonotonic transients, using an approach based on a model equation. To describe transient processes we start with a complete set of partial differential equations (PDE), which includes all known spatio-temporal processes inside of the detectors. Then, by estimating values of different terms in the complete set of equations, we will be able to neglect some of them to obtain a model tractable mathematically.

The continuity equation has the following form

$$p_t + j_x = -R; \tag{1}$$

$$R = gN((1-f)p - fp_1) \tag{2}$$

Send correspondence to:
T.H.: E-mail: tdh@ipac.caltech.edu (radhit detector)
E.H.: E-mail: engha@ipac.caltech.edu (stimflash calibration)
M.P.: E-mail: misha@ipac.caltech.edu (burger's equation)
D.K.: E-mail: dkelly@as.arizona.edu (data, algorithms)
G.R.: E-mail: grivlis@as.arizona.edu (data, algorithms)
C.E.: E-mail: chad@as.arizona.edu (data, algorithms)


Infrared Spaceborne Remote Sensing VIII, Marija Strojnik, Bjørn F. Andresen, Editors,
Proceedings of SPIE Vol. 4131 (2000) © 2000 SPIE · 0277-786X/00/$15.00

$$j = empE - eDp_x + eE_t \tag{3}$$

The Poisson's equation has the following form.

$$E_x = \frac{4\pi e}{\kappa}(N(f - f_0) + p - p_0) \tag{4}$$

The balance equation is written in the following form.

$$Nf_t = gN((1 - f)p - fp_1) \tag{5}$$

where $p(x,t)$ is the free hole concentration, $N$ is the concentration of traps, $f$ is the occupancy of traps, $R$ is the recombination rate, $m$ is the hole mobility, $D$ is the diffusion coefficient, $g$ is the coefficient describing the capture of electrons by traps, which is equal to the product of the capture cross section times $v_{th}$ thermal velocity, $p_1$ is the whole conduction density when the Fermi energy is equal to the energy of traps, $e$ is the electron charge, $\kappa$ is the permitivity, $E$ is the electric field applied along the $x$ axis, semiconductor. The expression for the hole current density $j$ includes possible contributions from drift, diffusion and displacement current components.

$$\frac{1}{\tau} = gN(1 - f_0) \tag{6}$$

is the reciprocal of the time governing the capture of free electrons by traps, and

$$\frac{1}{\tau_1} = \frac{p_0}{\tau N f_0(1 - f_0)} \tag{7}$$

is the reciprocal of the relaxation time of the occupancy of traps.

Assuming that a static electric field $E$ is applied along the $x$ axis and that the spatial and time variations of small perturbations in the hole concentration $p$, in the occupancy of traps, and in the electric field are proportional to $exp(ikx - i\omega t)$ we can linearize the system above and end up with the following dispersion relation for perturbations (see Kazarinov[2]).

$$\omega^2 - \omega[kv_0 - i(\frac{1}{\tau} + \frac{1}{\tau_1} + \frac{4p\sigma}{\kappa} + Dk^2)] - \frac{4p\sigma}{\kappa}(\frac{1}{\tau} + \frac{1}{\tau_1}) - \frac{i}{\tau_1}(kv_0 - iDk^2) = 0 \tag{8}$$

where $\sigma = emn$ is the conductivity, $v_0 = \mu E_0$. Let's first estimate the relative importance of the drift and diffusion. The diffusion length is

$$L_D = \sqrt{Dt} \gg 10^{-3.5} - 10^{-2.5} cm. \tag{9}$$

The drift length is

$$L_d = v_0\tau = 10^{-4} - 10^{-2} cm. \tag{10}$$

We have $D \gg 10^2 \frac{cm}{s}, v_0 \gg 10^5 \frac{cm}{s}$ (see Haegel[3]). For large enough $k \gg 10^4 \frac{1}{cm}$ we obtain the following root of the dispersion relation

$$w = v_0 k - iDk^2 \tag{11}$$

This dispersion relation corresponds to the linear Burgers equation. So, we see that, at least in linear approximation, there are two dominating physical effects: drift and diffusion. However, we would like to incorporate into our model the nonlinearity of the system. To do so, we will make use of the nonlinear Burger's equation, which takes into account nonlinear drift and diffusion together:

$$p_t + v_0 p_x + pp_x = Dp_{xx}, \tag{12}$$

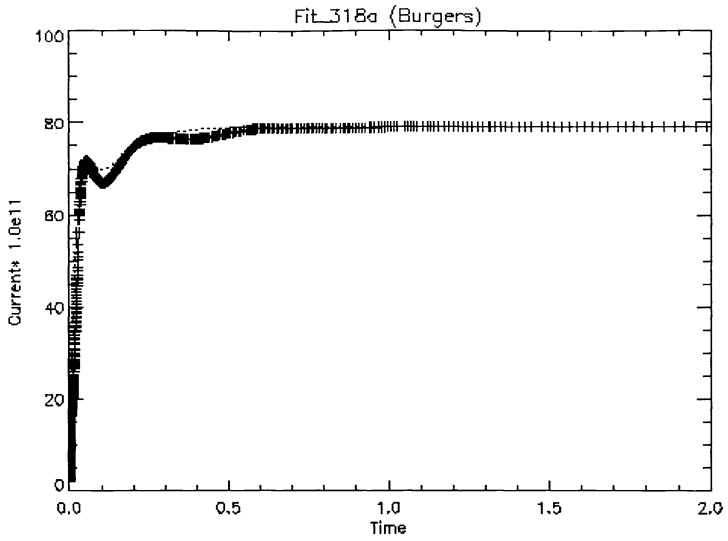


**Figure 1.** Fitting hook data to Burgers model. The actual asymptotic value is 79.1968, the fitting asymptotic value is 78.2068

Here we suggest a further simplification based on using a specific analytical solution of the Burgers equation. The solution has the following form.

$$p = p_1 + \frac{p_2 - p_1}{1 + bexp((p_2 - p_1)\frac{(x-Ut)}{2D})} \tag{13}$$

$$U = \frac{p_1 + p_2}{2} \tag{14}$$

In the fitting procedure the spatial variable $x$ is set to zero. These simplifications have been justified aposteriori by successful fitting to the experimental data.

### 1.2. Applications of the Burgers equation

Application of the Burgers equation to the problem of monotonic transients gives the asymptotic values identical to those obtained from the Fuks-Schubert model (the difference is less than 1percent). It also shows that by using only 30 percent of the real data, the asymptotic level can be predicted with the accuaracy 1.4 percent. The main advantage of the approach suggested here is the possibility of capturing the so-called hook effect. Figure 1 shows the result of the fitting to Burgers model hook-data numerically simulated by Haegel and Skoge.[4]

## 2. THE RADHIT DETECTOR

It is expected that, in the environment of space, the detector elements of SIRTF instruments will be exposed to charge-inducing events. While careful shielding will reduce the number of events, long integration times and the large detector areas required for detection at infrared wavelengths will lead to significant occurrence of radiation hits in the data. SIRTF integrations will be sampled several times during the observation. This will nominally produce a linear time series of charge from the detector readout. When a radiation hit occurs, there is an increase in the charge accumulated by the detector during the corresponding sampling interval. This results in a raising of the measured charge values at that and all suceeding samples. In this section is presented a method of detecting the resulting changepoint in the time series data. The method is not complicated to implement; matrices are involved, but can be calculated beforehand. After data collection, they are only used in matrix multiplication. Otherwise, most of the other computation consists of vector inner products, exponentiation of a scalar, and a sort process.

## 2.1. The probability distribution

The rise in charge at a detector element during a sampling interval of duration $\Delta t$ is dependent on the photon flux and the dark current of the detector. These two effects may be combined into a single rate, $\zeta$. Assuming that the combination of rate and sampling duration is high enough for the accumulation of about 15 electrons or more, the probability density function for the charge rise $\Delta E_t$ may be considered gaussian. It is

$$P(\Delta E_t|\not\gamma) = N(\zeta\Delta t, \zeta\Delta t, \Delta E_t) \tag{15}$$

where $N(\mu, \sigma^2, x)$ is a normal probability density over $x$ of mean $\mu$ and variance $\sigma^2$. The $t$ subscript in $\Delta E_t$ indicates the time at which the sample is taken. This index is most conveniently taken as ranging from 1 to $N$, where $N$ is the number of samples in the integration. The symbol $\not\gamma$, "gamma-slash", indicates that no radiation hit occurred.

The accumulated charge at time $T$ is the sum of all the charge increases up to $T$

$$E_{cum}(T) = \sum_{t<=T} \Delta E_t \tag{16}$$

No pedestal charge is assumed since it will not affect the calculations and in the end the quantity of interest is the slope of the charge vs time. The variance of $E_{cum}(T)$ is equal to $E_{cum}(T)$ and the expected value of the variance barring radiation hits is $\zeta T$. The read noise in electrons, $\sigma_{rn}$, adds gaussian noise to the measurement. Therefore the measured charge, $E(T)$, has an expected variance of $\zeta T + \sigma_{rn}^2$.

When a radiation hit occurs in the sample labeled $t$, it adds an amount $\Delta E_{rh}$ to the charge rise. Since there is currently no precise prediction of the distribution of $\Delta E_{rh}$ for SIRTF instruments, calculations in this report will be performed conservatively at a constant, low $\Delta E_{rh}$. Then the charge rise when a radiation hit occurs during the sample time with label $t$ obeys the probability density function

$$P(\Delta E_t|\gamma) = N(\zeta\Delta t + \Delta E_{rh}, \zeta\Delta t, \Delta E_t) \tag{17}$$

where the variance is as before. $\Delta E_{rh}$ does not contribute to the variance because it is assumed to be a constant. The symbol $\gamma$ indicates that a radiation hit occurred.

The accumulated charge at time $T$ follows the equation as above. Typically, the charge vs time data when one radiation hit occurs will consist of a linear segment as charge from photon flux and dark current is steadily accumulated, a discontinuous jump in charge at the sample at which the radiation hit occurs, and another linear segment of charge accumulation. Efforts to detect radiation hits will center on detecting the discontinuity in charge and determining whether it is statistically significant.

### 2.1.1. A Changepoint Detector

The following method is due to Kheradmandnia.[5]

### 2.1.2. The General Linear Model

Suppose that the data is linear except at the discontinuity where the radiation hit occurs, at time $t$. Then it could be fitted with a pair of linear functions,

$$E_{fit}(T) = a_1 + b_1 T \qquad when \qquad T < t \tag{18}$$

$$E_{fit}(T) = a_2 + b_2 T \qquad when \qquad T > t \tag{19}$$

The data need not have the same slope before and after the changepoint. Since there are a finite number of samples, the above equations can be written as:

$$\begin{aligned} E_{fit}(t_1) &= a_1 + b_1 t_1 \\ E_{fit}(t_2) &= a_1 + b_1 t_2 \\ E_{fit}(t_3) &= a_1 + b_1 t_3 \\ &\vdots \\ E_{fit}(t_{M-1}) &= a_1 + b_1 t_{M-1} \end{aligned} \tag{20}$$

$$
\begin{aligned}
E_{fit}(t_M) &= a_2 + b_2 T_M \\
E_{fit}(t_{M+1}) &= a_2 + b_2 T_{M+1} \\
&\vdots \\
E_{fit}(t_N) &= a_2 + b_2 T_N
\end{aligned}
$$

where the radiation hit occurs in the $M^{th}$ sample. $N$ is the total number of samples. The above can be written in matrix form

$$\mathbf{E_{fit}} = \mathbf{Gb} \tag{21}$$

where

$$\mathbf{G} = \begin{pmatrix} 1 & t_1 & 0 & 0 \\ 1 & t_2 & 0 & 0 \\ 1 & t_3 & 0 & 0 \\ \vdots & & & \\ 1 & t_{M-1} & 0 & 0 \\ 0 & 0 & 1 & t_M \\ 0 & 0 & 1 & t_{M+1} \\ \vdots & & & \\ 0 & 0 & 1 & t_N \end{pmatrix}$$

and

$$\mathbf{b} = \begin{pmatrix} a_1 & b_1 & a_2 & b_2 \end{pmatrix}^{\mathbf{T}}$$

If $\mathbf{E}$ represents the measured charges, and with the error defined from the following

$$\mathbf{E} = \mathbf{E_{fit}} + \mathbf{e} \tag{22}$$

then $\mathbf{E}$ satisfies the likelihood function

$$p(\mathbf{E}|\mathbf{G}, \mathbf{b}, \sigma) = (\mathbf{2\pi\sigma^2})^{\frac{N}{2}} \exp[-\frac{\mathbf{e^T e}}{\mathbf{2\sigma^2}}] \tag{23}$$

The data is assumed to be normal and of constant variance $\sigma$. This is an approximation to the noise expected in the measured charges, in which the photon noise, dark current fluctuations, and read noise are the main contributors. In the measured charges, the photon and dark current noise increase in proportion to the amount of charge accumulated, while the read noise remains constant.

Ó Ruanaidh and W.J. Fitzgerald[8] integrate the constants $\mathbf{b}$, and $\sigma$ out of the above equation to express the likelihood of a choice of $\mathbf{G}$ given the data

$$p(\mathbf{G}|\mathbf{E}) \propto \frac{[\mathbf{E^T E} - \mathbf{E^T G}(\mathbf{G^T G})^{-1}\mathbf{G^T E}]^{-\frac{(N-M)}{2}}}{\sqrt{\mathbf{det}(\mathbf{G^T G})}} \tag{24}$$

The method of determining the changepoint is to posit it to be at a chosen value $M$ and compute the likelihood of the corresponding $\mathbf{G}$, which contains the choice of $M$ implicitly. This is repeated for all possible $M$, and the result with the greatest likelihood is taken to indicate the location of the changepoint. A charge ramp of 80 samples with a slope of 900 electrons per sample and a readnoise of 120 electrons containing a radhit of magnitude 2000 electrons at sample number 52 is shown in figure 2, and a plot of the log of the likelihood, call it $L(M)$, vs $M$ for this charge ramp is shown in figure 3.

## 2.2. Declaring the Presence or Absence of a Radiation Hit

The method described assumes a priori that a radiation hit occurred, and estimates the most likely sample number of the hit. An additional procedure is needed in order to determine whether or not a radiation hit occurred. The procedure is based on a comparison of the charge increase at the location of the posited radiation hit compared to

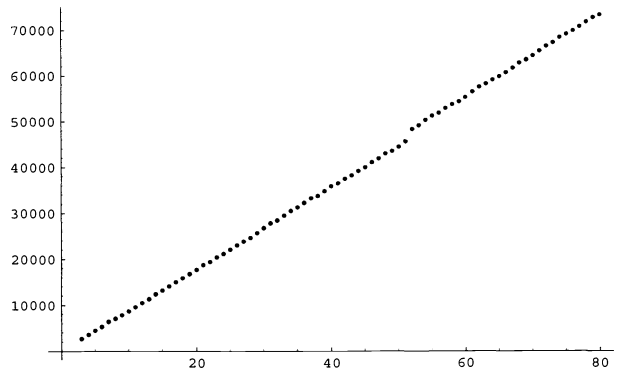


**Figure 2.** Charge vs sample number for ramp with 900 e/sample flux and radhit of 2000 at sample 52.

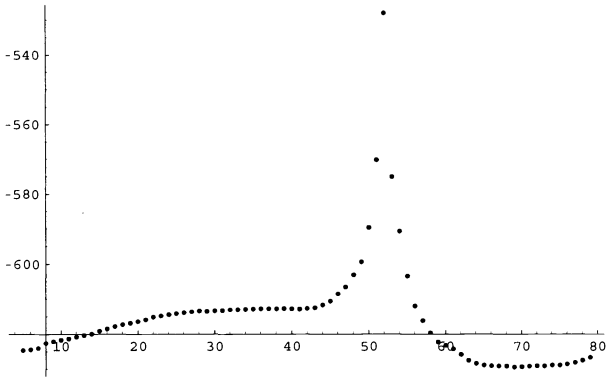


**Figure 3.** Log-likelihood vs sample number for charge ramp of previous figure 2.

the expected charge increase. Suppose that, from the calculation in section 2.1.2, the most likely changepoint is determined to be at $M$. The change in measured charge from $M-1$ to $M$ due to the radiation hit is

$$\Delta E_M = E_M - E_{M-1} - \zeta \Delta t \tag{25}$$

where the expected increase without a radiation hit $\zeta \Delta t$, due to dark current and the collection of photons, is subtracted off. A more accurate estimate of the charge increase is given by (eq. 21)

$$\Delta E_M = \mathbf{E}_{fit}(M) - \mathbf{E}_{fit}(M-1) - \zeta \Delta t \tag{26}$$

and the vector of least squared estimates is

$$\mathbf{E}_{fit} = \mathbf{G}(\mathbf{G}^{\mathbf{T}}\mathbf{G})^{-\mathbf{1}}\mathbf{G}^{\mathbf{T}}\mathbf{E} \tag{27}$$

Now it must be determined whether $\Delta E_M$ is large enough to be considered as resulting from a radiation hit. Bayes rule states that, given $\Delta E_M t$, the probability that a radiation hit occurred is,

$$P(\gamma|\Delta E_M) = \frac{P(\Delta E_M|\gamma)P(\gamma)}{P(\gamma) + P(\not\gamma)} \tag{28}$$

where the definitions of $P(\Delta E_M|\gamma)$ and $P(\Delta E_M|\not\gamma)$ are based on equations 17 and 15, with the difference that the variance due to the read noise is added to the variance parameter of the gaussian function. $P(\gamma)$ and $P(\not\gamma)$ are the a priori probabilities that a radiation hit did, and did not, occur, respectively. To complete the probability calculation, the charge accumlated due to flux and read noise during one sample period, $\zeta \Delta t$ in equations 15, 17, and 26, and the amount of charge added by the radiation hit, $\Delta E_{rh}$, in eq. 17 must be determined. The quantity $\zeta \Delta t$ is estimated from the data before the posited radiation hit:

$$\zeta_{est} \Delta t = \mathbf{E}_{fit}(M-1) - \mathbf{E}_{fit}(M-2) \tag{29}$$

and the magnitude of the radiation hit is taken as the lowest magnitude one could expect to detect at a high confidence level. This is expressed as a radiation hit magnitude to noise ratio $SNR_{min}$, times the expected standard deviation of the measured $\Delta E_M$. In other words,

$$\Delta E_{rh} = SNR_{min}\sqrt{\zeta_{est}\Delta t + \sigma_{rn}^2} \tag{30}$$

The quantity $\sqrt{\zeta_{est}\Delta t + \sigma_{rn}^2}$ is to be used as the standard deviation in $P(\Delta E_M|\gamma)$ and $P(\Delta E_M|\not\gamma)$. The quantity $SNR_{min}$ was set equal to three, which in the simulations produced a high probability of detection and an acceptable false alarm rate at all chosen values of flux and read noise.

| | | |
|---|---|---|
| $N$ | 80 | samples |
| $\sigma_{rn}$ | 120 | electrons |
| $\zeta$ | 900 | electrons per sample |
| $\Delta E$ | 0-2000 | electrons |

**Table 1.** Values of parameters used in simulations

## 2.3. Detecting Radiation Hits at the Endpoints

The likelihood calculation for $\mathbf{G}$ cannot be done for $M = 1,\ 2,\ or\ N$. Indeed, if the radiation hit occurs during the first sample, the very first and all subsequent charge measurements will contain the effect of the hit, and there will be no discontinuity in the data. Therefore no changepoint detection method can detect a radiation hit in the first sample. When $M = 2$ or $M = N$, the matrix $\mathbf{G}$ is singular and the method fails. To handle $M = 2$ or $M = N$, the data point at $M$ is examined directly in relation to the rest of the data. The method is similar for that used to determine the presence of a radiation hit as described in section 2.2. An estimate fof $\Delta E_M$ must be found, and it must be determined whether $\Delta E_M$ is large enough to be considered as resulting from a radiation hit.

### 2.3.1. The Matrix Method at the Endpoints

The method to be used will take advantage of the following fact: when a radiation hit occurs at $M = 2$ or $M = N$, the likelihood function $p(\mathbf{G}|\mathbf{E})$ has its maximum at $M = 3$ or $M = N - 1$, respectively. Therefore, whenever the method of section 2.1.1 yields $M = 3$ or $M = N - 1$ as the most likely changepoint location, the endpoints must be checked as candidates for the true changepoint location.

### 2.3.2. The Procedure for Examining the Far Endpoint

When the maximum of $p(\mathbf{G}|\mathbf{E})$ is at $M = N - 1$, the actual radhit, if any, could be at either $N - 1$ or $N$. Thus $\Delta E_M$ of eq. 26 is taken as the maximum of

$$\Delta E_N = \mathbf{E}_{fit}(N) - \mathbf{E}_{fit}(N-1) - \zeta_{est}\Delta t \tag{31}$$

and

$$\Delta E_{N-1} = \mathbf{E}_{fit}(N-1) - \mathbf{E}_{fit}(N-2) - \zeta_{est}\Delta t \tag{32}$$

Then the procedure from section 2.2 is then applied to determine whether a radiation hit should be declared.

### 2.3.3. The Procedure for Examining the Near Endpoint

When the maximum of $p(\mathbf{G}|\mathbf{E})$ is at $M = 3$, the actual radhit, if any, could be at either 2 or 3. The estimation of the flux from eq. 29 is

$$\zeta_{est}\Delta t = \mathbf{E}_{fit}(2) - \mathbf{E}_{fit}(1) \tag{33}$$

$\mathbf{E}_{fit}$ at the values 1 and 2 when $M = 3$ is a fit to a two-point data segment and thus $\zeta_{est}$ is very susceptible to noise in $E_1$ and $E_2$. Use of this value of $\zeta_{est}$ in eq. 30 would result in many misdeclarations. The slope is best estimated from the segment of the charge ramp after the radhit. There may be a radhit between samples 2 and 3, and so the following quantity is used:

$$\zeta'_{est}\Delta t = \mathbf{E}_{fit}(4) - \mathbf{E}_{fit}(3) \tag{34}$$

The threshhold from eq. 30 is then recalculated. This approach has the drawback of including data that occurs after the radiation hit. However, the radiation hit will still be detectable unless the new $\zeta'_{est}\Delta t$ is comparable to the charge addition due to the radiation hit itself. $\Delta E_M$ is then taken as the maximum of

$$\Delta E_2 = \mathbf{E}_{fit}(2) - \mathbf{E}_{fit}(1) - \zeta'_{est}\Delta t \tag{35}$$

and the value $\Delta E_3$ calculated from eq. 26. The procedure from section 2.2 is then applied with the appropriate flux estimate to determine whether a radiation hit should be declared.

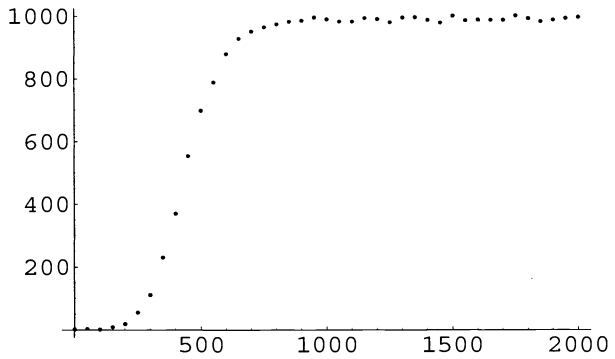


**Figure 4.** Number of correct declarations out of 1024 vs radhit magnitude with the probability threshold for declaring a radhit set to 0.99.

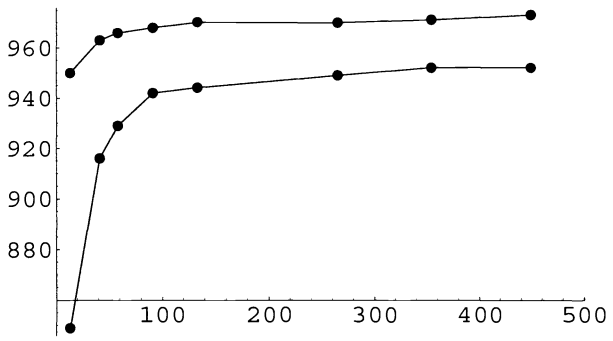


**Figure 5.** Number of correct declarations for two different radhit magnitudes vs number of false alarms for 1024 charge ramps.

## 2.4. Performance on Simulated data

There are several parameters to be set in the production of simulated data: the number of samples in the integration, $N$, the read noise, $\sigma_{rn}$, the charge flux due to photons and dark current, $\zeta$, whether or not a radiation hit occurred, and if so, its position, $M$, and its magnitude $\Delta E$. Table 1 shows the tested range of values of the parameters. The parameters were chosen to correspond to typical physical values for the 70 um detector.

For each value of $\Delta E$, 1024 charge ramps each containing exactly one radhit were prepared. The location of the radhit was chosen randomly from the range 2 to $N$. The radhit detector algorithm was performed on the ramps to obtain a probability and sample number for each one. Probabilities were compared to a threshold in order to declare a radhit, and a radhit declaration was considered correct only if the sample number was also correct. The radhit detector was operated with the a priori radhit probability $P(\gamma)$set to 0.4.

Figure 4 shows the number of correct declarations of the radhit detector vs magnitude when the threshold was 0.99. Reliable radhit detection begins at about 600 electrons. To optimize the threshold, the radhit magnitude was held constant and the threshold was varied. At each threshold, the number of false alarms (declarations for the $\Delta E = 0$ ramps) was tabulated. For each threshold, the number of correct detections was also counted and plotted against the number of false alarms. Figure 5 shows the resulting plots for two radhit magnitudes, 600 electrons (lower curve) and 750 electrons (upper curve). The probability threshold for declaring a radhit is the parameter for each curve and takes on the values, from left to right, (0.999, 0.995, 0.99, 0.975, 0.95, 0.85, 0.75, 0.65) . The plots show that a threshold of 0.99 gives the best tradeoff of probability of detection vs probability of false alarm.

## 2.5. Performance on Real data

A 70 um detector array of 4 x 32 elements was placed in the proton beam of a synchrotron and 45 charge ramps were measured. The charge ramps were 64 samples long, each sample being about 1/8 second in duration. The background illumination level was such as to produce a response in the detector of about 2000 electrons per second. In addition, a second stimulator was flashed every 18 charge ramps for a duration of two charge ramps at a level of 10,000 electrons per second.

Since more than one radhit event can occur in a single charge ramp, the radhit detector was executed multiple times on each charge ramp. If a radhit was found in a charge ramp, the radhit detector was executed again on each of the two segments defined by the radhit, and so on. There is no a priori knowledge of whether a given charge ramp contains a radhit and therefore a direct measure of radhit detector performance cannot be done. Figure 6 shows the frequency of the number of radhits found per charge ramp. The curve shows that the frequency obeys a power law as expected, and that the radhit detector can reliably detect multiple radhits up to seven per charge ramp.

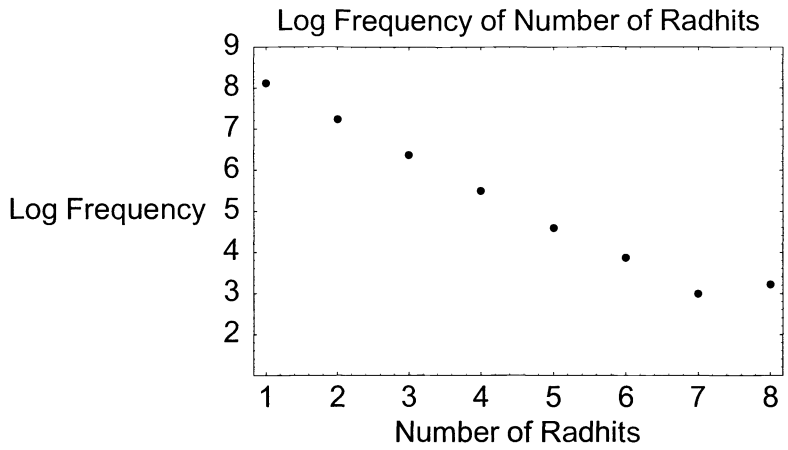


**Figure 6.** Log frequency plot of the number of radhits found per charge ramp.

## 3. STIMFLASH CALIBRATION

Each pixel in the MIPS Germanium array has a responsivity that depends on its internal physical characteristics and the previous impinging flux history. Pixel responsivity also tends to rise with accumulated cosmic ray dose. The responsitivity change will have many undesirable effects; among them are: (a)the pixel response will appear to be not proportional to the incident flux, and (b) the image will have artifacts that are NOT related to the objects in the observation.

To minimize the effects described above, a procedure has been devised whereby at regular intervals, an internal stimulator is excited to add a constant infra-red signal to the incident signal. These periodic stimflashes can then be used to deduce the relative instantaneous responsitivity of each pixel in the MIPS array. The stimflash calibration is complete when the resulting relative reponsitivity is applied to calibrate the measurements .

### 3.1. Theory and Assumptions

At a given Data Collection Event (DCE) $n$, we have a background flux $b(n)$ impinging on a pixel. If the responsitivity of the pixel is $h(n)$, then the measured response is

$$y(n) = h(n)b(n) \tag{36}$$

If some DCEs $dn$ later a constant stimflash flux $S$ is turned on to add to the background flux, then the measured response is

$$y_s(n + dn) = h(n + dn)[S + b(n + dn)] \tag{37}$$

If we assume that during this short interval $dn$ that the responsitivity is constant at $h(n)$ and the background flux $b(n + dn)$ is the same as $b(n)$, then

$$y_s(n + dn) - y(n) = h(n)S \tag{38}$$

Hence the instantaneous responsivity of the pixel is given by

$$h(n) = \frac{y_s(n + dn) - y(n)}{S} \tag{39}$$

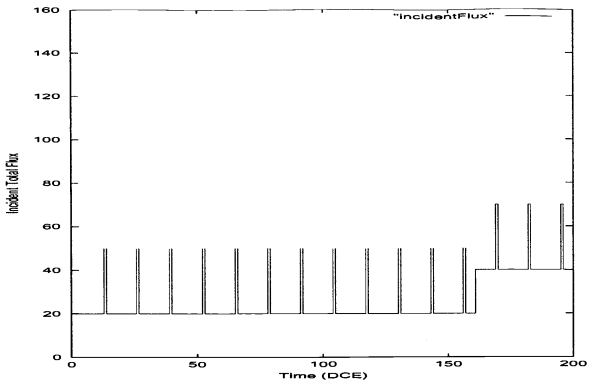


**Figure 7.** Total incident flux versus time showing stimflash every thirteenth DCE.

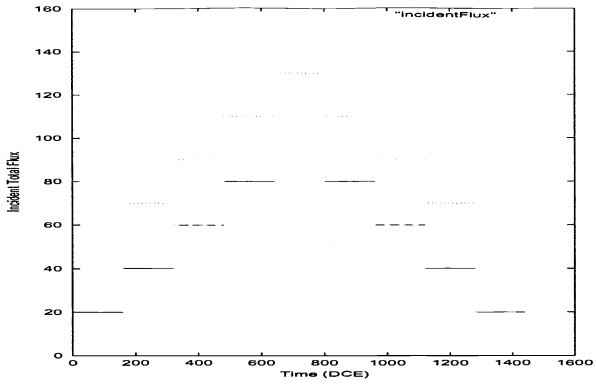


**Figure 8.** History of total incident flux history for the Aug 19 1999 experiment.

And the background flux can thus be calibrated by

$$b(n) = y(n)/h(n) = \frac{Sy(n)}{y_s(n+dn) - y(n)} \tag{40}$$

From the above, it can be seen that the stimflash measurement subtracted from the background measurement (stim - background) is the responsitivity calibration factor we can apply to individual pixels to remove the artifacts caused by internal characteristics of the MIPS array. In equation 3.1, the value of S shall be known in physical units (e.g., Jy) from comparison to a standard star measurement.

### 3.2. August 19 1999 Experiments

A three-hour long set of experiments was designed to verify the ability of our stimflash calibration to properly account for the responsivity changes in individual pixels. It consists of maintaining a background level for the duration of 160 Data Collection Events( DCE) and changing the background level and repeating the experiments. Each DCE consisted of 64 samples taken at a sampling interval of approximately $\frac{1}{8}$ second.

A stimulator flash is turned on for every 13th DCE. This is shown in figure 7. In this same figure it can be seen that the background flux is increased after being held constant for 160 DCEs.

Figure 8 depicts the incident flux history for the duration of the experiment. The solid horizontal lines are the background fluxes which changes every 160th DCE. The dotted lines are the stimflash-on-background fluxes at every 13th DCE. The background flux change is positive and uniform for the first half of the experiment and negative for the second half, thus retracing the changes of the first half.

The experiments were conducted on August 19, 1999 at the University of Arizona's Steward Observatory.

### 3.3. Measurements and Calibrated Results

Figure 10 shows the measured flux history for a pixel at row 20 and column 21. This flux is the slope of the least squares linear fit to the measured charge ramp. The first 15 samples of the charge ramp were discarded to reduce intra-DCE nonlinearity; in addition, radhits have been removed and saturated data discarded. It can be observed that the pixel responsitivity has changed with time such that there is a significant difference in response between the earlier measurements and the latter measurements for the same incident flux level.

Figure 9 shows the measured stim - background flux that is derived from figure 10. To prevent the significant noise present in this data from contaminating the calibration process, a least squares quadratic fit is performed and the fitted curve is shown as a solid line. The coefficients of the fit are then used to interpolate the needed stim - background data at every DCE. The measured flux is then calibrated according to equation 3.1 discussed earlier.

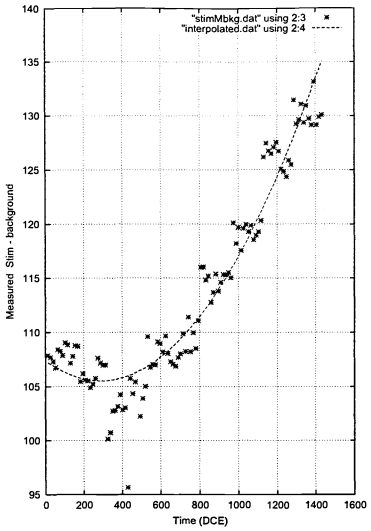


**Figure 9.** Measured Stim - Background flux vs time for pixel (20,21) with least squares quadratic fit.

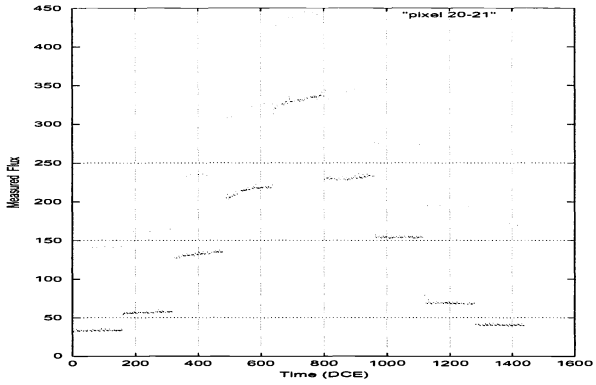


**Figure 10.** Measured flux versus time for Pixel 20-21

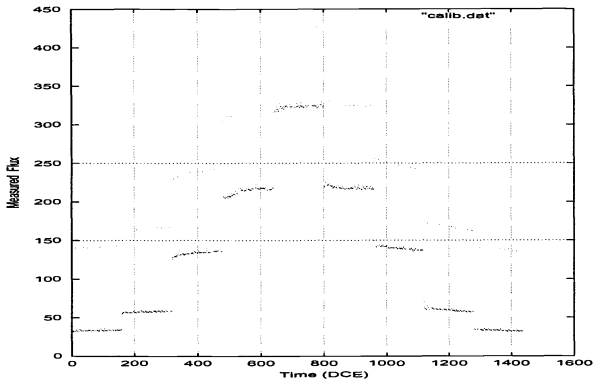


**Figure 11.** Stimflash calibrated total flux versus time for Pixel 20-21.

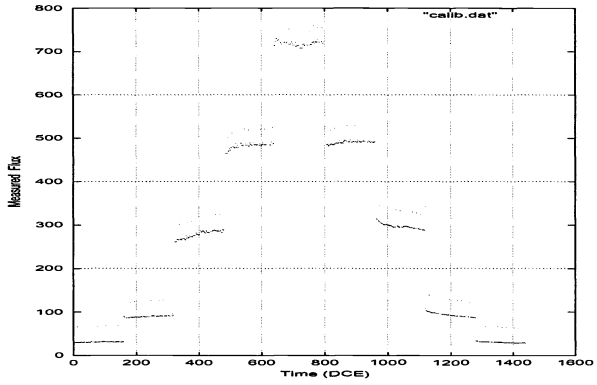


**Figure 12.** Stimflash calibrated total flux versus time for Pixel 16-16.

Figure 11 shows the calibrated flux history for pixel 20-21. Comparing this with the uncalibrated flux history, it can be seen that significant portion of the effects of pixel responsitivity change has been removed: namely , for the same incident flux,the response is almost the same for the long three hour duration of this experiment.

We have applied the same procedure to a large fraction of the pixels in the array. Similar results have been observed. For demonstration, the results for pixel16-16 are presented in figure 12.

### 3.4. Discussions and Future Work

Despite the amount of noise in the stimflash - background data, it can be concluded that the stimflash calibration approach works reasonably well for our August 19 1999 experiment lasting approximately three hours. It can be observed in the calibrated data that the long time scale curve fitting adopted here has introduced short time scale artifacts. Significant improvements and optimizations in the MIPS array have since been made and more data have been gathered in the new array. Some preliminary results are shown in Figure 14 for pixel 20-21 and Figure 13 for pixel 16-16. Here the stimflash - background is interpolated between two adjacent stimflashes to provide the calibration for

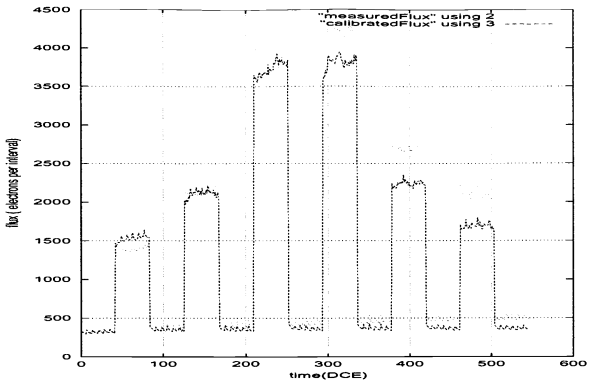


**Figure 13.** Measured and Calibrated Flux for Pixel 16-16

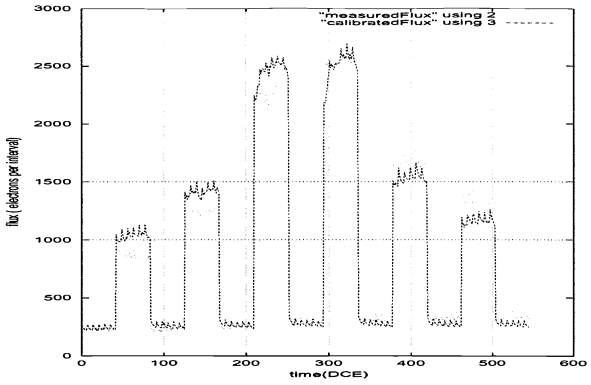


**Figure 14.** Measured and Calibrated Flux for Pixel 20-21

the background flux between the two stimflashes. The incident flux history is symmetrical in time about the center of the plot. It can be seen that the calibrated fluxes are much more symmetrical than the uncalibrated fluxes. More work needs to be done to understand some of the transients seen here and to then implement a more sophisticated stimflash calibration approach so that we can achieve a much higher degree of accuracy.

## ACKNOWLEDGMENTS

We gratefully acknowledge the participation of Mehrdad Moshir and George Rieke in all aspects of the MIPS project.

## REFERENCES

1. G. B. Heim, M. L. Henderson, K. I. Macfeely, T. J. McMahon, D. Michika, R. J. Pearson, G. H. Rieke, J. P. Schwenker, D. W. Strecker, C. L. Thompson, R. M. Warden, D. A. Wilson, and E. T. Young, "Multiband imaging photometer for SIRTF," in *Proc. SPIE: Space Telescopes and Instruments V*, P. Y. Bely and J. B. Breckinridge, eds., vol. 3356, pp. 985–1000, 1998.
2. R.Kazariniv, R.Suris, and B.Fuks, "Waves of spatial charge exchange," *Soviet Physics, Semiconductors* **7**(1), pp. 102–107, 1973.
3. N.Haegel, C.Latasa, and A.White, "Transient response of infrared photoconductors," *Applied Physics* **A56**, pp. 15–21, 1993.
4. N.Haegel and J. Skoge, "Simulation of transient behavior in extrinsic photoconductors: Modulated source modeling," Tech. Rep. Report for PY278651, Department of Physics, Fairfield University, Fairfield, CT, August 1999.
5. M. Kheradmandnia, *Aspects of Bayesian threshhold autoregressive modelling.* PhD thesis, University of Kent, England, 1991.
6. J. O. Ruanaidh and W. Fitzgerald, "The identification of changepoints using the bayesian general piecewise linear model," Tech. Rep. CUED/F-INFENG/TR134 (1993), Cambridge University Engineering Department, England, March 1994.
7. J. O. Ruanaidh, W. Fitzgerald, and K. J. Pope, "Recursive bayesian location of a discontinuity in time series," in *IEEE Int. Conf. on Acoustics, Speech and Signal Processing*, vol. IV, pp. 513–516, April 1994.
8. J. O. Ruanaidh and W. Fitzgerald, *Numerical Bayesian Methods Applied to Signal Processing*, Statistics and Computing Series, Springer Verlag, 1996.
9. D. Stephens, "Bayesian retrospective multiple changepoint identification," technical report series, Imperial College Mathematics Dept., Statistics Section, London, England, 1992.
10. D. Stephens, "Bayesian retrospective multiple-changepoint identification," *Applied Statistics* **43**, pp. 1159–1178, 1994.
11. J. Yates, *Changepoint detection using Bayesian inference.* PhD thesis, Cambridge University Engineering Department, England, 1994.